Author Manuscript
Accepted for publication in a peer-reviewed journal

NIST National Institute of Standards and Technology • U.S. Department of Commerce

Published in final edited form as:
CIRP Ann Manuf Technol. 2016 ; 65(1): 377–380. doi:10.1016/j.cirp.2016.04.117.

Diagnostics for geometric performance of machine tool linear axes

Gregory W. Vogl[a,*], **M. Alkan Donmez**[a], and **Andreas Archenti**[b]

[a]Engineering Laboratory, National Institute of Standards and Technology (NIST), 100 Bureau Drive, Gaithersburg, MD 20899-8220, USA[1]

[b]Department of Production Engineering, KTH Royal Institute of Technology, Brinellvägen 68, 10044 Stockholm, Sweden

Abstract

Machine tools degrade during operations, yet knowledge of degradation is elusive; accurately detecting degradation of linear axes is typically a manual and time-consuming process. Manufacturers need automated and efficient methods to diagnose the condition of their machine tool linear axes with minimal disruptions to production. A method was developed to use data from an inertial measurement unit (IMU) for identification of changes in the translational and angular errors due to axis degradation. A linear axis testbed, established for the purpose of verification and validation, revealed that the IMU-based method was capable of measuring geometric errors with acceptable test uncertainty ratios.

Keywords

Machine tool; Error; Diagnostics

1. Introduction

Machine tool linear axes move the cutting tool and workpiece to their desired positions for parts production [1]. A typical machine tool has multiple linear axes, and their accuracies directly impact the quality of manufactured parts. However, over a machine tool's lifetime, emerging faults lead to performance degradation, lowering accuracy and repeatability [2]. Typical sources of errors within feed drive systems are due to pitting, wear, corrosion, and cracks of the system components such as guideways and recirculating balls [3]. As degradation increases, tool-to-workpiece errors increase that eventually may result in a failure and/or a loss of production quality [4]. Yet knowledge of degradation is illusive; proper assessment of axis degradation is often a manual, time-consuming, and potentially cost-prohibitive process.

While direct methods for machine tool performance evaluation are well-established [5] and reliable for position-dependent error quantification, such measurements typically interrupt

*Corresponding author: gvogl@nist.gov (G.W. Vogl).

production [6]. An online condition monitoring system for linear axes is needed to help achieve decreased machine downtime, higher productivity, higher product quality, and enhanced knowledge about manufacturing processes [7]. Efforts to monitor the condition of linear axes components have utilized various sensors, e.g., built-in rotary encoders [8], current sensors [4], and accelerometers [9,10]. These attempts at condition monitoring of linear axes were limited in success, partly because of the lack of robustness and defined relationships of signals to axis degradation composed of a wide range of spatial frequencies.

One potential solution for online monitoring of linear axis degradation is the use of an inertial measurement unit (IMU). As seen in Fig. 1, an IMU is mounted to a moving machine tool component. To diagnose axis degradation, the axis is moved back and forth at various speeds to capture data for different bandwidths. This data is then ‘fused’ to estimate the changes in the 6-degree-of-freedom (DOF) geometric errors of the axis. Because the linear axes are stacked, coordinate transformations may be used with all 6-DOF errors to estimate the errors at the functional point [5]. Ideally, data would be collected periodically to track axis degradation with minimal disruptions to production. With robust diagnostics and prognostics algorithms, incipient faults may be detected and future failures may be avoided. In essence, IMU data can be used to help optimize maintenance, production planning, and ultimately part quality.

Following the approach outlined in Fig. 1, this paper introduces a novel IMU-based method for diagnostics of machine tool linear axes. A linear axis testbed was designed to physically implement the custom IMU and the IMU-based method. Various degradation patterns were experimentally simulated by adjustments of a guideway rail or defects imparted on bearing balls. This paper outlines the major findings of these experiments, revealing the potential of the novel IMU-based approach for diagnostics and prognostics of machine tools.

2. Testbed setup

A testbed was designed for evaluation of the IMU-based method. As seen in Fig. 2(a), the testbed includes a linear axis, the IMU, a commercial laser-based system for measuring the geometric errors of the axis, and a direct current (DC) motor with encoder for motion control. While the metrology system measures the motion of the carriage with respect to the base of the linear axis, the carriage-mounted IMU measures the changes in the inertial motion of the carriage. The commercial metrology system is able to measure straightness and angular error motions over the travel length of 0.32 m with standard uncertainties of 0.7 μm and 3.0 μrad. The laser-based system is used for verification and validation (V&V) of the IMU-based results.

For the detection of both translational and rotational motions, the IMU contains three accelerometers and one triaxial rate gyroscope, as seen in Fig. 2(b). Table 1 outlines key specifications of the IMU sensors. Each sensitive direction is nominally aligned with either the *X*-, *Y*-, or *Z*-axis of the testbed coordinate system. Consequently, these sensors enable the estimation of 6-DOF motion.

3. IMU-based method

As outlined in Fig. 1, the IMU-based method relies on sensor data collected during a fixed-cycle test, in which an axis is programmed to move unloaded at three constant speeds: Fast speed (v_1 = 0.5 m/s), moderate speed (v_2 = 0.1 m/s), and slow speed (v_3 = 0.02 m/s). Constant speeds allow for simple correlation of error motions with axis position while minimizing transient dynamic effects. The different speeds allow for sensing of repeatable error motions, composed of low to high spatial frequencies, within different temporal bandwidths. Such a process takes advantage of the enhanced signal-to-noise and lower sensor drift at faster speeds, while taking advantage of the detection of higher spatial frequencies at slower speeds without violating sensor bandwidths. As seen in Fig. 1, matching the spatial cutoff frequencies enables the data fusion, while filtering allows for the attenuation of significant modal excitations, especially resulting from the initial and final accelerations during the fast speed cycle.

For the linear axis testbed, data is collected while the carriage moves back and forth sequentially at each of three speeds for 50 runs. Data collection for multiple runs allows averaging for convergence purposes. Once data is collected, data fusion follows.

3.1. Angular motions

Data fusion for estimation of angular motions is represented in Fig. 3. Rate gyroscope data for three speeds is integrated once, low-or band-pass filtered, processed, and summed to yield the total angular motions following the scheme in Fig. 3(a).

In contrast, the scheme in Fig. 3(b) may also be used to estimate the angular motions about the *X*- and *Y*-directions. Measuring down to 0 Hz (see Table 1), the three accelerometer signals (A_X, A_Y and A_Z) for the *X*-, *Y*-, and *Z*-directions relate to the inclination angles (θ_X and θ_Y) as approximately [11]

$$A_X = a_X - g\theta_Y \quad (1a)$$

$$A_Y = a_Y + g\theta_X \quad (1b)$$

$$A_Z = a_Z - \frac{1}{2}g\left(\theta_X^2 + \theta_Y^2\right) \quad (1c)$$

where g is the magnitude of acceleration due to gravity. Thus, Eqs. (1a) and (1b) yield the respective inclinations, θ_Y and θ_X, when the accelerations (a_X and a_Y) are negligible. However, the data fusion scheme in Fig. 3(b) may not be applied for the *Z*-axis, for which no 'inclinometer' exists.

3.2. Translational motions

Data fusion for estimation of translational error motions is represented in Fig. 4. The accelerometer data is integrated twice, low- or band-pass filtered, processed, and summed to yield the net translational motions. Similar to the schemes in Fig. 3, the scheme in Fig. 4 relies upon the matching of spatial cutoff frequencies and the exclusion of significant modal excitations.

One main element of the processing utilized for the scheme in Fig. 4 involves accounting for corruptive effects due to inclinations as described by Eqs. (1a) and (1b). For the ith accelerometer, three signals are collected ($A_{i,1}$, $A_{i,2}$, and $A_{i,3}$) per run, one for each speed. Each signal may be represented as

$$A_{i,n} \approx f_i(x) + a_{i,n}(t) \quad (2)$$

where $f_i(x)$ is the common inclination-related component as a function of position, x, not of time, t. Eq. (2) is integrated in time and related to position as $V_{i,1}(x)$, $V_{i,2}(x)$, or $V_{i,3}(x)$. Eq. (2) is then applied for two speeds (fast and moderate, or moderate and slow) to isolate the acceleration, $a_{i,n}(x)$, due to common geometric error motions, resulting in Eqs. (3a) and (3b).

$$\frac{d}{dx}(v_1 V_{i,1}(x) - v_2 V_{i,2}(x)) \approx \left[1 - \left(\frac{v_2}{v_1}\right)^2\right] a_{i,1}(x) \quad (3a)$$

$$\frac{d}{dx}(v_2 V_{i,2}(x) - v_3 V_{i,3}(x)) \approx \left[1 - \left(\frac{v_3}{v_2}\right)^2\right] a_{i,2}(x) \quad (3b)$$

Eqs. (3a) and (3b) are used to isolate accelerations for the ‘Fast’ and ‘Moderate’ regimes in Fig. 4.

4. Convergence and general results

The data fusion method is not very useful without convergence. Fig. 5 shows the typical convergence of an estimated straightness error motion and an estimated angular error motion with increasing number of runs for averaging. The errors are labelled per the convention in ISO 10791-1 [12]. As seen in Fig. 5, 10 runs is usually sufficient for convergence within 5 μm or 15 μrad, which means the IMU-based method has the potential to estimate geometric motion errors with a test uncertainty ratio (TUR) of at least 4:1 per ISO 10791-1 [12].

In addition to convergence, the estimated error motions should match those of the laser-based commercial system. Fig. 6 compares the laser-based and IMU-based results; the standard deviations of the differences are 11 μm, 2.3 μm, and 13 μrad for the linear positioning, straightness, and angular error motions, respectively. Lower-frequency

deviations are partly due to thermal drift, since the reference and IMU data were not collected simultaneously. Higher-frequency deviations are partially due to the fact that IMU-based results are averaged for multiple runs, while laser-based results are not; differences include non-repeatable error motions.

However, due to the quadratic terms in Eq. (1c), the data fusion method is not robust for straightness error motions in the Z-axis direction. The quadratic nonlinearity implies that high-frequency angular vibrations cause low-frequency sensor offsets, which cannot be eliminated via Eq. (3a). One possible solution is to modify the IMU via rotation of the X- and Z-axis accelerometers about the Y-axis (see Fig. 2), such that all accelerometer signals depend linearly on angular motions as in Eqs. (1a) and (1b).

5. Experiments

Two experiments were performed to investigate the ability of the IMU-based method to resolve low- and high-frequency components of error motions.

In the first experiment outlined in Fig. 7(a), a linear axis rail was deformed with shims to simulate low spatial frequency degradations of a machine tool axis. The entire rail was raised with shims so that the centre shims could be changed without loosening more than one screw (the centre rail screw). The systematic change in centre height to 38 μm is evidenced in the change of the angle about the Y-axis, as seen in Fig. 7(b). Low spatial frequency changes over 200 μrad dominate the response with insignificant differences in high-frequency components among the curves of Fig. 7(b).

In the second experiment outlined in Fig. 8, bearing balls within a truck were degraded to simulate high spatial frequency degradations of a machine tool linear axis. Thirty-two balls of a truck were degraded via the abrasive removal of material, one ball at a time, resulting in defects in the form of flattened rougher surfaces as shown in Fig. 8(a). Case 0 in Fig. 8 is the nominal case of Grade 25 chrome steel balls with no defects (nominal diameter = 3.981 mm). For each subsequent case, one extra defect was created on each ball at a random location, and the additional defect was of a greater nominal size. Defects ranged in depth from 3 μm to 10 μm. Consequently, differences are dominated by high-frequency terms among the curves of Fig. 8(b) once DC shifts (due to loosening/tightening of testbed screws between cases) are neglected.

6. Conclusions

Manufacturers need efficient and automated methods for diagnosis of machine tool linear axes with minimal disruptions to production. Towards this end, an inertial measurement unit and associated data fusion method were developed for machine tool application. The IMU-based method uses data from both accelerometers and rate gyroscopes to identify changes in translational and angular error motions due to axis degradation. Data is fused in the spatial frequency domain via filtering in order to include both low- and high-frequency error motions while excluding significant modal excitations.

The IMU-based method was verified and validated via a testbed containing a linear axis and a laser-based system for measurement of the geometric axis performance. The IMU-based results typically converge within 5 μm or 15 μrad when using 10 runs for averaging, needed for the estimation of changes in geometric motion errors with test uncertainty ratios of at least 4:1. Several experiments showed that the IMU-based method is capable of resolving both low- and high-frequency error motion components. Measurement results are prone to variations in system noise, but the method incorporates averaging along with convergence testing to accommodate increased noise.

Future application of the IMU-based method on machine tools will require the IMU to be mounted on the stacked axes. Possible limitations may include varying sensitivity to wear and cross-talk among the stacked axes. Final conformance of the method to a particular machine tool will require additional testing to adjust the spatial cutoff frequencies for data fusion and overcome these possible limitations.

Because the method is robust for the detection of defects, appropriate diagnostic metrics based on this method can be defined to facilitate industrial applications. Such metrics would use the IMU-based data to quantify machine tool linear axis degradation, and to inform the user of the magnitude and location of wear and any violations of performance tolerances. Further tests may show the value of additional metrics for prognostic purposes to estimate the remaining useful life of linear axes performance. Finally, if the data collection and analysis are integrated within a machine controller, the process may be streamlined for the optimization of maintenance, supporting the development of self-diagnosing smart machine tools.

References

1. Altintas Y, Verl A, Brecher C, Uriarte L, Pritschow G. Machine Tool Feed Drives. CIRP Annals – Manufacturing Technology. 2011; 60(2):779–796.
2. Li Y, Wang X, Lin J, Shi S. A Wavelet Bicoherence-Based Quadratic Nonlinearity Feature for Translational Axis Condition Monitoring. Sensors. 2014; 14(2):2071–2088. [PubMed: 24473281]
3. Zhou, Y., Mei, X., Zhang, Y., Jiang, G., Sun, N. Current-Based Feed Axis Condition Monitoring and Fault Diagnosis. 4th IEEE Conference on Industrial Electronics and Applications, ICIEA; 2009; 2009. p. 1191-1195.
4. Uhlmann E, Geisert C, Hohwieler E. Monitoring of Slowly Progressing Deterioration of Computer Numerical Control Machine Axes. Proceedings of the Institution of Mechanical Engineers Part B: Journal of Engineering Manufacture. 2008; 222(10):1213–1219.
5. International Organization for Standardization. ISO 230-1 – Test Code for Machine Tools – Part 1: Geometric Accuracy of Machines Operating Under No-Load or Quasi-Static Conditions. 2012.
6. Khan, AW., Chen, W. Calibration of CNC Milling Machine by Direct Method. 2008 International Conference on Optical Instruments and Technology: Optoelectronic Measurement Technology and Applications; 2009. p. 716010
7. Teti R, Jemielniak K, O'Donnell G, Dornfeld D. Advanced Monitoring of Machining Operations. CIRP Annals – Manufacturing Technology. 2010; 59(2):717–739.
8. Verl A, Heisel U, Walther M, Maier D. Sensorless Automated Condition Monitoring for the Control of the Predictive Maintenance of Machine Tools. CIRP Annals – Manufacturing Technology. 2009; 58(1):375–378.
9. Liao L, Lee J. A Novel Method for Machine Performance Degradation Assessment Based on Fixed Cycle Features Test. Journal of Sound and Vibration. 2009; 326(3–5):894–908.

10. Spiewak S, Zaiss C, Ludwick SJ. High Accuracy, Low-Invasive Displacement Sensor (Halids). ASME 2013 International Mechanical Engineering Congress and Exposition, IMECE 2013, 2A:V02AT02A077. 2013

11. McConnell, KG., Varoto, PS. Vibration Testing: Theory and Practice. 2. John Wiley & Sons, Inc; Hoboken, New Jersey: 2008. p. 174-180.

12. International Organization for Standardization. ISO 10791-1 – Test Conditions for Machining Centres – Part 1: Geometric Tests for Machines with Horizontal Spindle and with Accessory Heads (Horizontal Z-Axis). 2014.

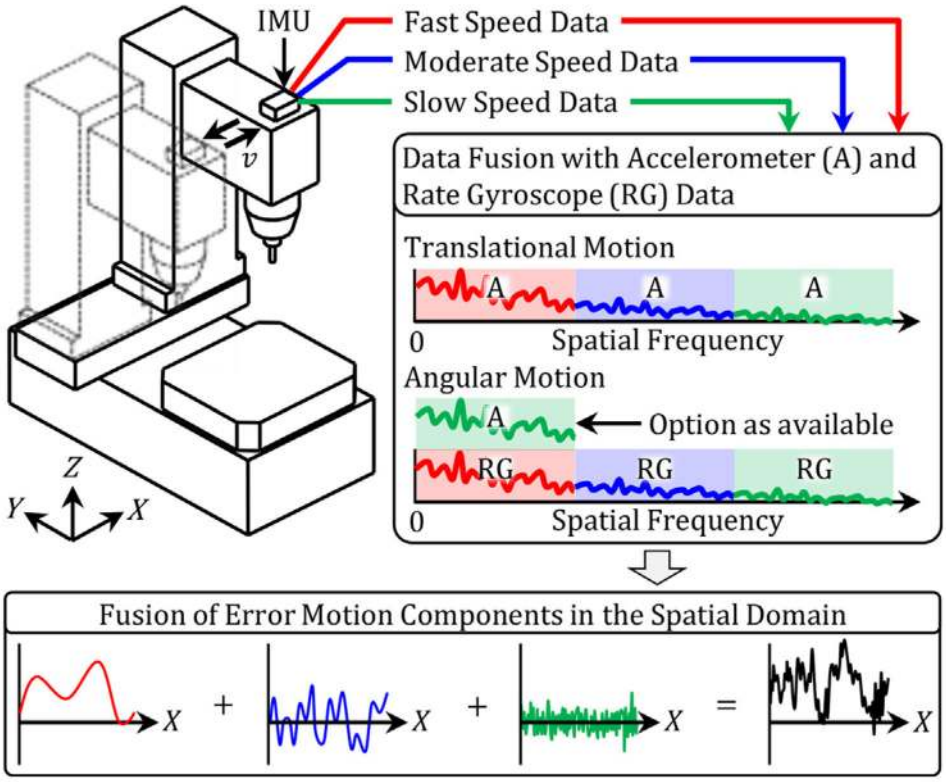

Fig. 1.
IMU-based method for diagnostics of machine tool performance degradation.

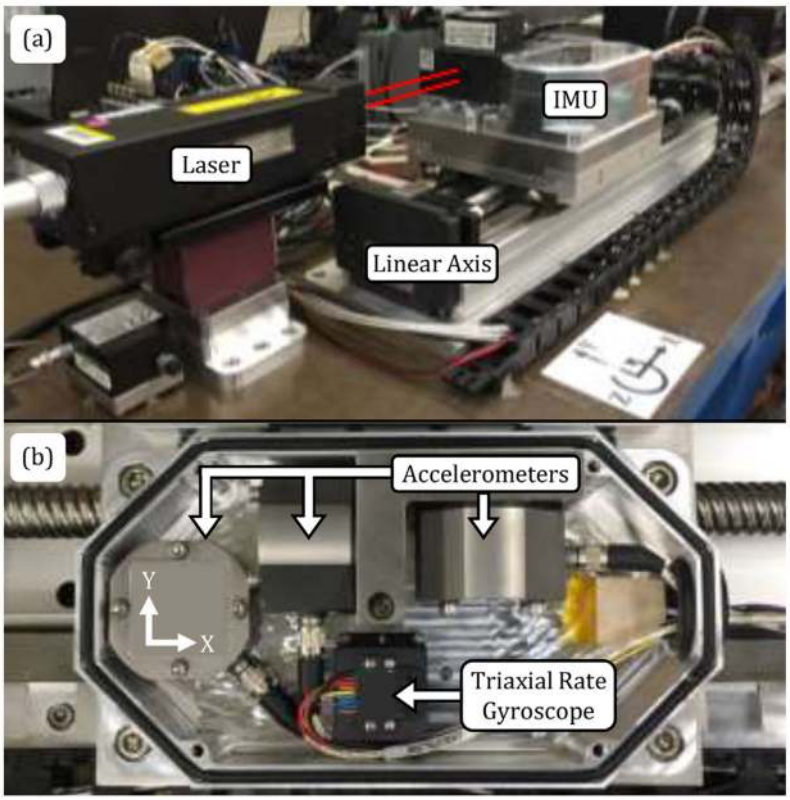

Fig. 2.
(a) Linear axis testbed and (b) top view of IMU without its lid.

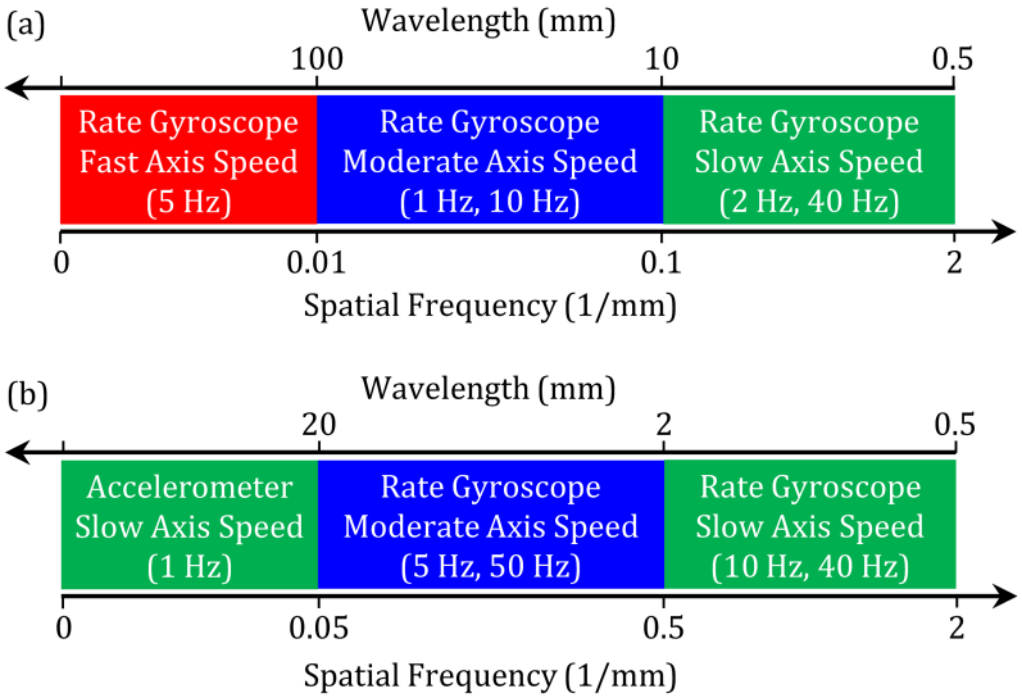

Fig. 3.

Data fusion scheme for angular motions via use of (a) rate gyroscope data or (b) accelerometer and rate gyroscope data. Filter cutoff frequencies are shown in parentheses.

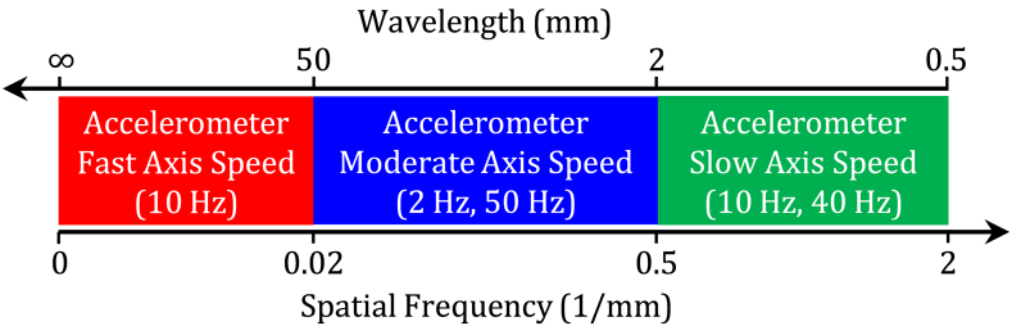

Fig. 4.

Data fusion scheme for translational motions via use of accelerometer data. Filter cutoff frequencies are shown in parentheses.

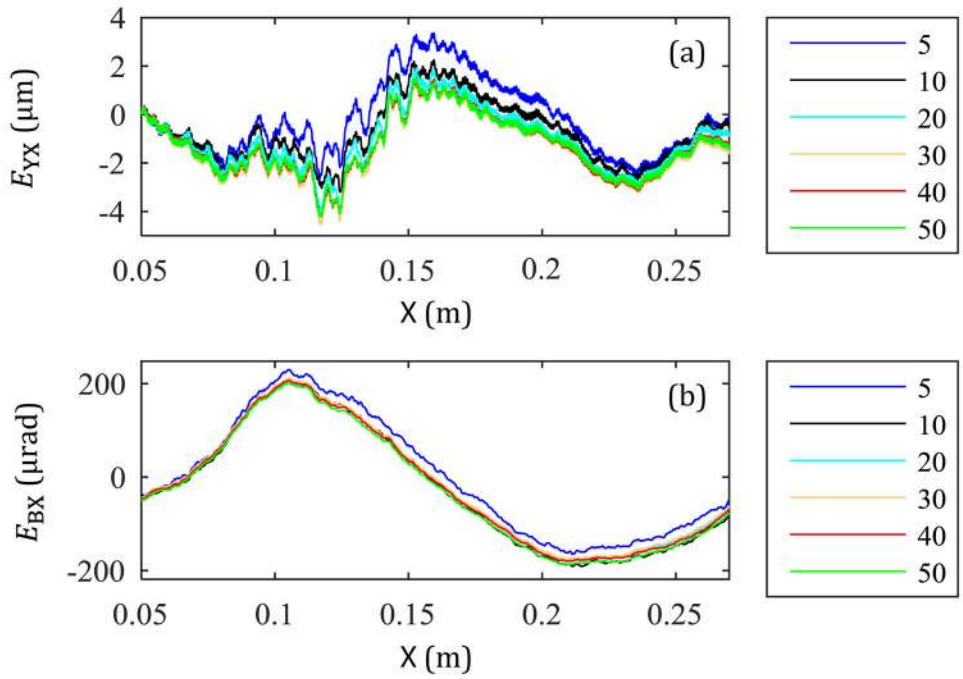

Fig. 5.

Typical convergence of (a) an estimated straightness error motion (via accelerometer data) and (b) an estimated angular error motion (via rate gyroscope data) with increasing number of runs for averaging.

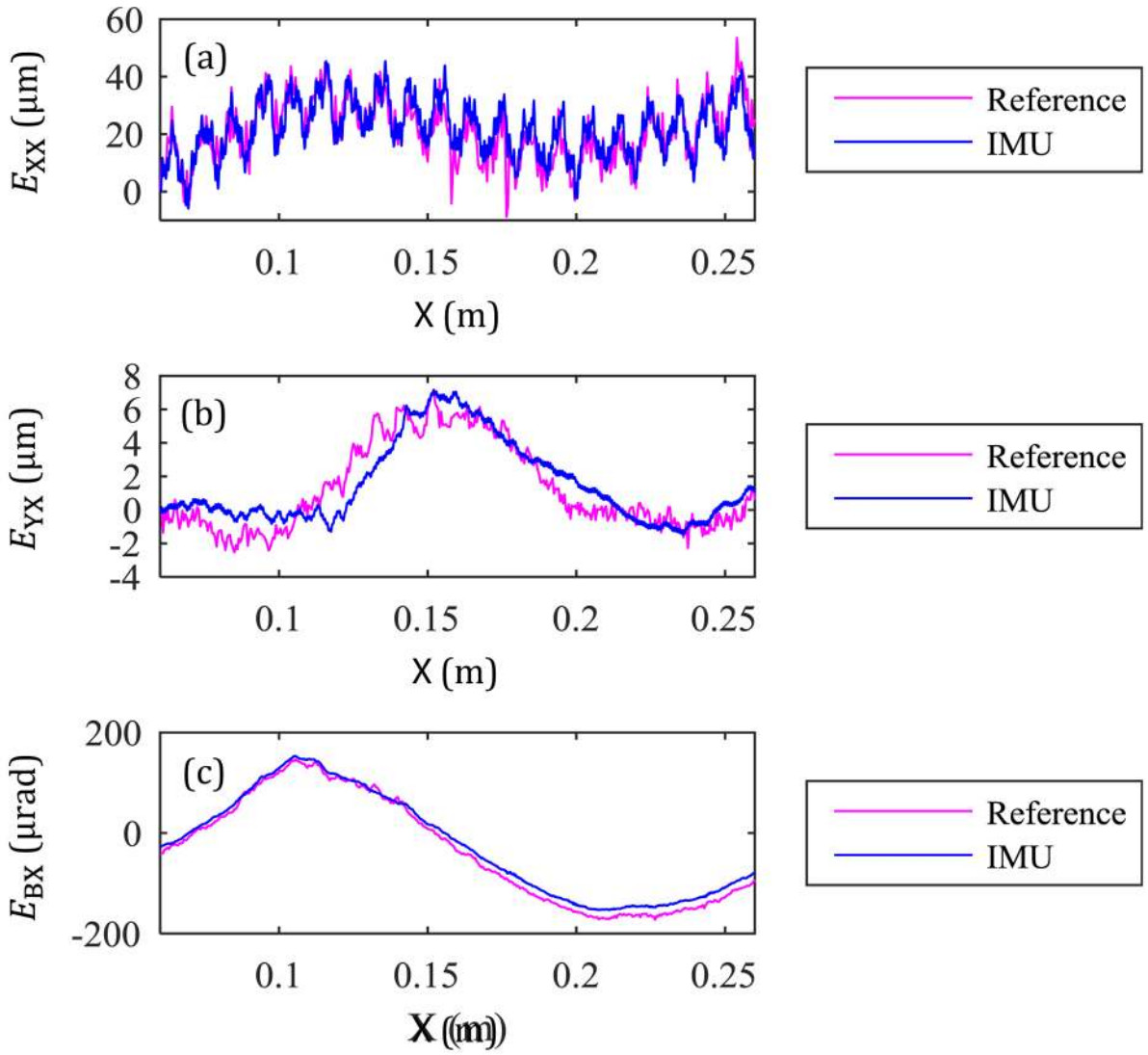

Fig. 6.

Example of converged (a) linear positioning error motion, (b) straightness error motion, and (c) angular error motion for various sensing methods.

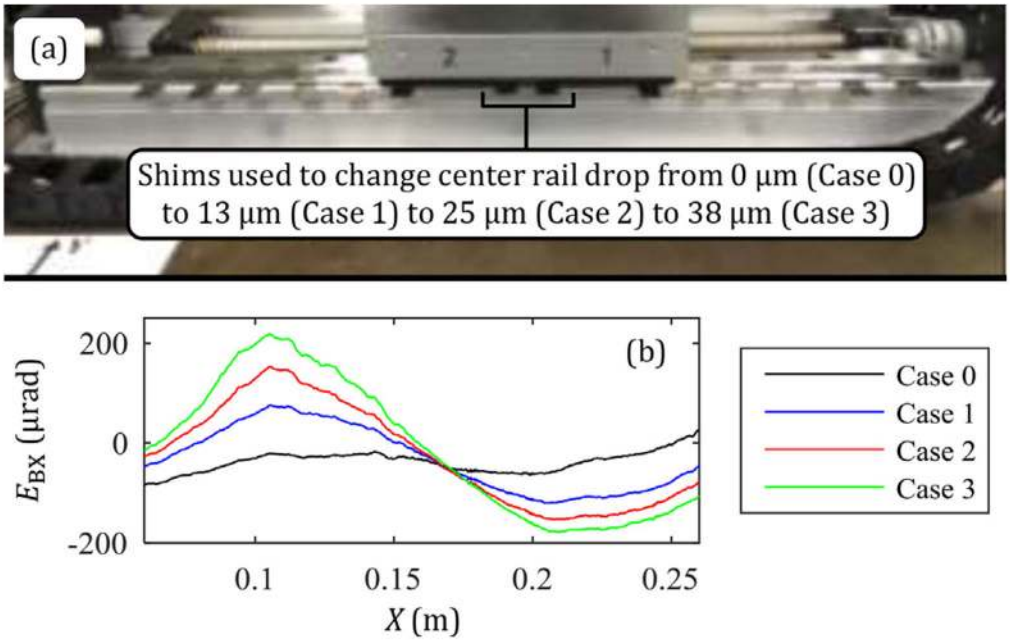

Fig. 7.

(a) Experimental setup to represent low-frequency degradations of a guideway rail, resulting in (b) changes in pitch error motion (E_{BX}) observed by IMU (data averaged for 50 runs).

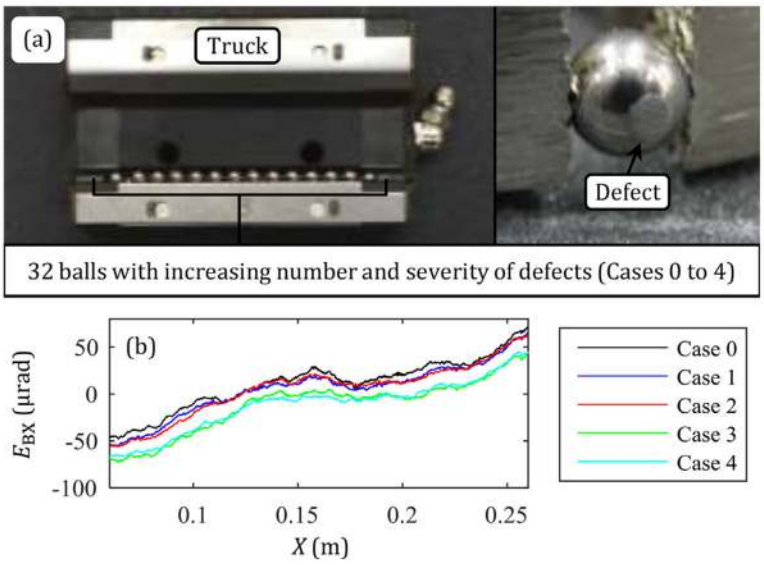

Fig. 8.

For high-frequency degradations due to defects of bearing balls, (a) 32 balls of a truck were degraded via the abrasive removal of material, resulting in (b) changes in pitch error motion (E_{BX}) observed by IMU (data averaged for 50 runs).

Table 1

Specified properties of sensors used in the IMU.

Sensor	Bandwidth[a]	Noise
Accelerometer	0–1800 Hz	4.0 (μm/s^2)/$\sqrt{\text{Hz}}$ from 0 Hz to 100 Hz
Rate gyroscope	0–200 Hz	35 (μrad/s)/$\sqrt{\text{Hz}}$

[a]Frequencies correspond to half-power points, also known as 3 dB points.